Geomorphology 121 (2010) 15–21

Contents lists available at ScienceDirect

Geomorphology

journal homepage: www.elsevier.com/locate/geomorph

# Modeling aeolian sediment transport thresholds on physically rough Martian surfaces: A shear stress partitioning approach

John A. Gillies [a,*], William G. Nickling [b], James King [c], Nicholas Lancaster [d]

[a] Division of Atmospheric Sciences, Desert Research Institute, 2215 Raggio Parkway, Reno NV 89512, USA
[b] Wind Erosion Laboratory, Department of Geography, University of Guelph, Guelph ON, Canada N1G 2W1
[c] Division of Atmospheric Sciences, Desert Research Institute, 755 E. Flamingo Road, Las Vegas, NV 89119, USA
[d] Division of Earth and Ecosystem Sciences, Desert Research Institute, 2215 Raggio Parkway, Reno NV 89512, USA

ARTICLE INFO

*Article history:*
Received 21 May 2008
Received in revised form 15 December 2008
Accepted 6 February 2009
Available online 20 February 2009

*Keywords:*
Aeolian sediment transport thresholds
Shear stress partitioning
Mars

ABSTRACT

This paper explores the effect that large roughness elements (0.30 m×0.26 m×0.36 m) may have on entrainment of sediment by Martian winds using a shear stress partitioning approach based on a model developed by Raupach et al. (Raupach, M.R., Gillette, D.A., Leys, J.F., 1993. The effect of roughness elements on wind erosion threshold. Journal of Geophysical Research 98(D2), 3023–3029). This model predicts the shear stress partitioning ratio defined as the percent reduction in shear stress on the intervening surface between the roughness elements as compared to the surface in the absence of those elements. This ratio is based on knowledge of the geometric properties of the roughness elements, the characteristic drag coefficients of the elements and the surface, and the assumed effect these elements have on the spatial distribution of the mean and maximum shear stresses. On Mars, unlike on Earth, the shear stress partitioning caused by roughness can be non-linear in that the drag coefficients for the surface as well as for the roughness itself show Reynolds number dependencies for the reported range of Martian wind speeds. The shear stress partitioning model of Raupach et al. is used to evaluate how conditions of the Martian atmosphere will affect the threshold shear stress ratio for Martian surfaces over a range of values of roughness density. Using, as an example, a 125 μm diameter particle with an estimated threshold shear stress on Mars of ≈0.06 N $m^{-2}$ (shear velocity, $u_* \approx 2$ m $s^{-1}$ on a smooth surface), we evaluate the effect of roughness density on the threshold shear stress ratio for this diameter particle. In general, on Mars higher regional shear stresses are required to initiate particle entrainment for surfaces that have the same physical roughness as defined by the roughness density term (λ) compared with terrestrial surfaces mainly because of the low Martian atmospheric density.



## 1. Introduction

Aeolian sediment entrainment and transport processes play an important role in the evolution of the Martian landscape. The most dramatic demonstration of aeolian activity on Mars is the planet-wide dust storm (Gierasch, 1974; Martin and Zurek, 1993), although dust storms on the scale of $>10^2$ $km^2$ to $>10^6$ $km^2$ are more frequent. Data presented by Martin and Zurek (1993) and more recently by Cantor et al. (2001) indicate dust storms are a common occurrence on Mars. The presence of wind-derived bedforms on Mars, such as, sand sheets, ripples, megaripples and sand dunes provide further evidence of aeolian activity. In addition to smaller scale aeolian bedforms, which are observed in plains areas (Sullivan et al., 2005) evidence exists of sand entrainment and transport in areas among roughness elements ranging in size from pebbles to boulders (Jakosky and Christensen, 1986). This surface type has been imaged by the Mars Exploration Rover Mission (http://marsrovers.jpl.nasa.gov/home/). These surfaces are areas where it can be expected that the presence of the roughness create conditions whereby entrainment of sediments by wind requires increased wind speeds compared to the aerodynamically smoother plains.

This paper explores the effect that larger roughness elements may have on entrainment of sediment by Martian winds using a shear stress partitioning approach based on a model developed by Raupach et al. (1993). The Raupach et al. (1993) model predicts the shear stress partitioning ratio defined as the percent reduction in shear stress on the intervening surface between the roughness elements as compared to the surface in the absence of those elements (Wolfe and Nickling, 1993). This ratio is based on knowledge of the roughness element geometric properties, the characteristic drag coefficients of the elements and the surface, and the assumed effect these elements have on the spatial distribution of the mean and maximum shear stresses.

Recent work by King et al. (2005) and field testing by Gillies et al. (2006, 2007) have demonstrated that this model can effectively predict roughness effects on entrainment threshold for terrestrial

* Corresponding author.
*E-mail address:* jackg@dri.edu (J.A. Gillies).

0169-555X/$ – see front matter © 2009 Elsevier B.V. All rights reserved.
doi:10.1016/j.geomorph.2009.02.016

atmospheric conditions. Thompson et al. (2004) have also applied this model to predict the effects of roughness on shear stress partitioning in a fluvial environment. As the model can be used for different fluid properties, it is possible to evaluate how the atmospheric conditions and winds of Mars interact with the roughness and affect sediment entrainment on this planet. Sullivan (2002) discussed application of shear stress partitioning to estimate effects on the threshold of entrainment by Martian winds at the Pathfinder landing site, but he did not fully consider the dependency effects of the Reynolds number that will be very important in the thin Martian atmosphere. In this paper the results of Gillies et al. (2007), which provide data on the effect large solid roughness elements of varying roughness density have on shear stress partitioning and particle threshold and aerodynamic parameters, are used in the Raupach et al. (1993) shear stress partitioning model to evaluate how Martian atmospheric conditions could affect the entrainment of 125 μm diameter particles positioned among roughness elements on Martian surfaces. Sullivan et al. (2005) suggest that this particle size diameter represents an upper limit of sand size observed in local depressions at the Meridiani Planum landing site. In this paper we will evaluate the effect of Martian atmospheric conditions on particle entrainment for the same range of roughness densities evaluated by Gillies et al. (2006, 2007) in terrestrial field tests of aeolian sediment entrainment and transport in New Mexico, USA (refer to Fig. 1, Gillies et al., 2007 for images of the roughness configurations for which detailed shear stress partitioning data are available). Finally, based on available estimates of roughness density for Mars drawn from the literature, estimates of threshold wind speeds, required to mobilize this same size particle for these rough surfaces, will be presented.

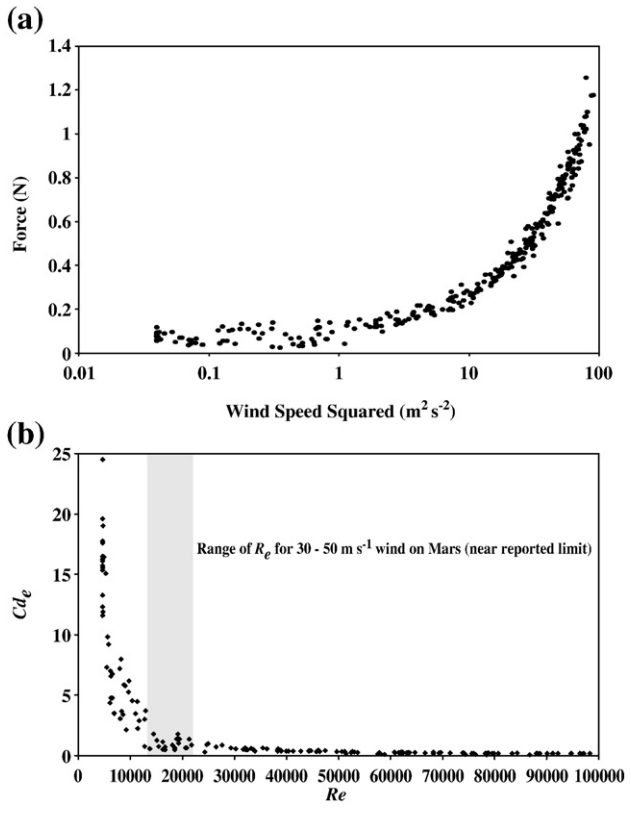


**Fig. 1.** (a) The relationship between force ($F$, $N$) and wind speed squared ($m^2\ s^{-2}$) for the modeled roughness element (Gillies et al., unpublished data). (b) Drag curve for the surface mounted roughness element based on the data from (a) and the experiments of Gillies et al. (2006, 2007). The shaded area for the $Re$ range 12,780 to 21,300 indicates the range of $Re$ associated with published estimates of maximum surface wind speeds of 30 m $s^{-1}$ to 50 m $s^{-1}$ on Mars, based on observation (Leovy, 2001). On Earth independence of $Cd_e$ from $Re$ is expected at $Re \geq 2\times10^4$.

## 2. Background

Research to explain the physics of the threshold of sediment transport by wind on Mars was presented in a series of landmark papers beginning with the work of Sagan and Pollack (1969) and Hess (1973). Following on from this work the laboratory simulations of Martian conditions in a specialized low pressure wind tunnel by Greeley et al. (1976, 1980), Iversen et al. (1976) and Iversen and White (1982) resulted in a comprehensive understanding of the controls on particle entrainment by the fluid drag forces exerted by wind and retarding effects of inter-particle forces. This work produced threshold curves that relate the minimum wind shear velocity ($u_*$, m $s^{-1}$) needed to raise particles of different sizes from the Martian surface. Shear velocity is proportional to the shear stress ($\tau_0\,[N\,m^{-2}] = \rho_a u^2_*\,[m\,s^{-1}]$, where $\rho_a$ is atmospheric density [kg $m^{-3}$]) imposed on the surface by the turbulent atmospheric boundary layer, which is critically influenced by the surface roughness. Gravity and inter-particle forces also influence the threshold of entrainment. The particle threshold curves for Mars, derived by Greeley et al. (1980), however, are based on wind shear stress exerted by boundary layer winds blowing over relatively uniform and aerodynamically smooth surfaces.

According to Gillette (1999), non-erodible roughness exerts the greatest influence on particle entrainment threshold for the erodible material among the roughness elements. These non-erodible elements absorb momentum that would otherwise be transferred to the surface if they were absent. It is, therefore, critical to account for the effect of roughness on aeolian particle threshold. The effect of roughness on particle threshold is controlled by how the drag forces and shearing stresses are partitioned between the roughness elements and the intervening surface (Schlichting, 1936). As the quantity of roughness elements is increased, total drag and roughness drag increase while the force acting on the intervening surface among the roughness decreases. Although the shear stress required to entrain a particle of a certain size is relatively invariant, as roughness increases it takes a greater amount of shear stress in the total flow to reach the amount of force on the intervening surface necessary to mobilize that particle.

Raupach (1992) provided a detailed re-evaluation of shear stress partitioning and brought it into the context of wind erosion and sediment entrainment and transport by wind. He defined the partitioning of the total shear stress ($\tau_0$) of a rough surface, as stated by Schlichting (1936) (i.e., $\tau_0 = \tau_S + \tau_R$, where $\tau_S$ is the shear stress on the intervening surface among the roughness elements and $\tau_R$ is the shear stress associated with the roughness), in terms of surface and element drag coefficients, roughness density, wind speed at a reference height, and wind shear velocity. This model defines the partition of drag in terms of a shear stress ratio ($R_t$) of the threshold for sediment entrainment for the bare surface in question to the threshold of the surface including roughness. The lower the value of $R_t$ the greater the protection that is offered by the roughness to the intervening surface.

Subsequent to the original model of Raupach (1992), Raupach et al. (1993) identified several perceived shortcomings and modified the model by adding two terms; the first defines an aspect ratio while the second delineates the threshold of the surface by some undefined function of the maximum stress instead of the average stress. This redefinition is essential in the context of wind erosion and dust emission in that the threshold of a surface is not a function of an averaged stress but a maximum stress (Stout and Zobeck, 1997). The Raupach et al. (1993) shear stress partition model is expressed as:

$$R_t = \left(\frac{\tau''_S}{\tau}\right)^{1/2} = \left(\frac{1}{(1-m\sigma\lambda)(1+m\beta\lambda)}\right)^{1/2} \quad (1)$$

where $\tau''_S$ is the maximum stress, $\sigma$ is defined as the ratio of the basal to frontal area, $m$ is a parameter between 0 and 1 that accounts for the

spatial and temporal variations in the stress on the intervening surface. The $\beta$ term is defined as the ratio of the drag coefficient of a single roughness element ($Cd_e$) to that of the surface without elements ($Cd_s$). Raupach et al. (1993) suggest a value of 0.5 for $m$ for a flat, erodible surface and a value that approaches one for an erodible surface that is quasi-stable with equilibrium bed topography. Lambda, or the roughness density ($\lambda$), is a dimensionless number used to characterize the roughness element size, numbers, and surface area the elements are distributed within and is expressed as:

$$\lambda = \frac{nbh}{S} \tag{2}$$

where $n$ is the number of roughness elements of width $b$ and height $h$ per unit surface area ($S$).

One of the main assumptions in the Raupach (1992) and Raupach et al. (1993) approach is that the roughness is modeled as a solid object. This assumption allows for the further simplification of the drag reduction behind an individual roughness element because it expresses an area with no stress and over the rest of the surface, a time-averaged uniform stress. Behind a porous object such as a plant, however, a gradient of drag reduction occurs that is continually changing in time and space. Unlike on Earth, all non-erodible roughness on Mars is non-porous making direct application of this model appropriate to Martian conditions.

## 3. Application of the SSR model to Martian conditions

The atmosphere of Mars has some similarity with the atmosphere on Earth and some striking differences (Larsen et al., 2002). The temperature regimes of the two planets overlap with the Martian range reported to be −125 to +25 °C while Earth has a range between −80 and +50 °C. Because a larger fraction of the solar radiation reaches the surface of Mars than it does on Earth, they have similar net radiation environments (Larsen et al., 2002). Notable differences in atmospheric conditions between the planets are found in the compositions, pressures, and densities. The atmosphere of Mars is mainly composed of carbon dioxide, whereas nitrogen and oxygen dominate on Earth. The surface pressure of Mars is <0.01% of the surface pressure of Earth, while the typical surface densities of the atmospheres are $1.5\times10^{-2}$ kg m$^{-3}$ and 1.2 kg m$^{-3}$ for Mars and Earth, respectively. The kinematic viscosity of the atmosphere on Mars is typically $10^{-3}$ m$^2$ s$^{-1}$ while for Earth it is $1.5\times10^{-5}$ m$^2$ s$^{-1}$ (at a temperature of 220 K and 300 K for Mars and Earth, respectively).

The application of the Raupach et al. (1993) shear stress partitioning model to Martian conditions depends critically on whether the known scaling laws for atmospheric processes on Earth apply equally on Mars. According to Larsen et al. (2002), terrestrial scaling laws largely apply on Mars making the transference of the Raupach et al. (1993) model a reasonable assumption. For estimating sediment transport thresholds it will be critical to have knowledge of the shearing stress at the surface. Larsen et al. (2002) indicate that it is safe to assume that the characteristic velocity scale $u_*$, from which $\tau_0$ can be estimated, is the same on Mars and Earth.

The shear velocity is defined in the logarithmic law (Prandtl, 1935), which defines the wind speed relationship as a function of height in the inertial sublayer (ISL) under neutral conditions, and is expressed as:

$$\frac{u_z}{u_*} = \frac{1}{\kappa}\ln\left(\frac{z-d}{z_o}\right) \tag{3}$$

where $u_z$ is wind speed at height $z$ (m), $\kappa$ is the von Kármán constant (0.4), $z_o$ is aerodynamic roughness length (m), and $d$ is the displacement height (m) (Jackson, 1981). Gillies et al. (2007) could not estimate with any confidence that a displacement height was present for any of the surfaces they measured, which is also assumed to be the case if roughness of similar $\lambda$ (i.e., $0.016<\lambda<0.095$) occurred on Mars.

As a result of the low atmospheric density of Mars several circumstances arise such that the shear stress partitioning response is likely distinctly different than that observed on Earth. The greatest effects of Martian atmospheric and surface conditions on the partitioning of shear stress at the surface, as defined by Eq. (1), are manifested through the drag coefficient ratio, $\beta$.

On Earth the drag coefficient of a surface mounted roughness element can be defined as:

$$Cd_e = F/(\rho_a A_f u_z^2) \tag{4}$$

where $F$ is the force (N) exerted on the element by the fluid flow and $A_f$ is element cross sectional area (m$^2$). On Earth, $Cd_e$ becomes independent of flow Reynolds number ($Re$) at relatively low wind velocities. Reynolds number here is defined as:

$$\mathrm{Re} = \frac{\rho_a u h}{\mu} \tag{5}$$

where $h$ is element height, and $\mu$ is atmospheric (dynamic) viscosity (kg m s$^{-1}$). Unlike the drag coefficients for objects falling (or being towed) through still fluids that reach independence from $Re$ at ≈1000, wall-mounted bluff bodies submerged in a thick turbulent boundary can exhibit dependencies on $Re$ to values of $2–3\times10^4$ (Lim et al., 2007).

The relationship between force (N) and wind speed squared (m$^2$ s$^{-2}$) (Fig. 1a, Gillies et al., unpublished data) for the roughness element used to construct the rough surfaces studied by Gillies et al. (2007) along with the drag curve for this roughness element (Fig. 1b) are shown in Fig. 1. The roughness elements used were five gallon plastic buckets (0.26 m×0.30 m×0.36 m) with the form being a slightly tapering cylinder, so that the projected frontal area form was an isosceles trapezoid. The force data required to solve Eq. (5) were obtained by having the element mounted on a drag balance and in isolation on an open flat surface with wind speed measured by a nearby anemometer (~1.5 m away) mounted at 0.36 m above ground level (Gillies et al., 2006, 2007). The non-linear response of the force versus wind speed squared below approximately 10 m$^2$ s$^{-2}$ (Fig. 1a), indicates conditions where $Cd_e$ is dependent on $Re$ (Fig. 1b).

Independence of $Cd_e$ from $Re$ was observed to occur at $Re$ values >75,000 (corresponding to a wind speed ≥3 m s$^{-1}$ at 0.36 m above ground level) for this surface-mounted roughness element on Earth, which is greater than the expected range of $2–4\times10^4$. This may reflect limitations of the drag balance instrument used by Gillies et al. (2007). The shaded area on Fig. 1b for the $Re$ range 12,780 to 21,300, indicates the range of $Re$ associated with published estimates of maximum surface wind speeds of 30 m s$^{-1}$ to 50 m s$^{-1}$ on Mars, based on observation (Leovy, 2001), which suggests that roughness elements on the surface of Mars can be expected to have drag coefficients that show dependency on $Re$ up to these wind speeds.

A variable $Cd_e$ results in a variable shear stress partitioning ratio, which is distinctly different from terrestrial surfaces, creating a non-linearity in the shear stress partitioning process on Mars over a wide range of wind speed.

The surface drag coefficient ($Cd_s$) for the intervening surface, or the surface in the absence of large roughness elements, is the second component of the $\beta$ term that could have a variable value on Mars over a greater range of wind speed. This results from its dependence on $u_*$ over a much greater range than would be found on Earth. $Cd_s$ can be defined as (Kondo and Yamazawa, 1986; Mahrt et al., 2001):

$$Cd_s = (\kappa/\ln(z/z_o))^2 \tag{6}$$

Kondo and Yamazawa (1986) observed that $Cd_s$ exhibited dependence on $u_*$, and hence $\tau_0$, when the roughness Reynolds number, defined as:

$$\mathrm{Re_R} = \rho_a u_* h/\mu \quad (7)$$

was $<\approx 17$ and in a smooth flow regime. Iversen et al. (1976) determined that particle threshold shear velocity was also dependent on $Re_R$ in a low $Re_R$ regime. In this case the roughness elements are subsumed within the laminar sublayer (von Kármán, 1954). As $u_*$ or roughness size increases, form drag becomes important in addition to skin friction, but in the transitional regime defined as $17<Re_R<63$, $Cd_s$ remains dependent on $u_*$ and/or the element roughness height. In the completely rough regime, form drag is greater than skin drag, and the flow is independent of the $Re_R$.

## 4. Modeling threshold as a function of roughness on Mars for a 125 μm diameter particle

To evaluate how the entrainment of a 125 μm diameter mineral grain is affected by the roughness that surrounds it on Mars, we begin with the following assumptions: 1) the threshold shear stress in the absence of large roughness (i.e., a smooth surface) on Mars is 0.06 N $m^{-2}$ ($u_{*t}\approx 2.0$ m $s^{-1}$) (Iversen and White, 1982), 2) the roughness on Mars is of the same size and shape, and is arranged into the same configurations as that used by Gillies et al. (2007), 3) the $Cd_e$ relationship as a function of flow $Re$ is defined by Fig. 1b, 4) the surface on which the particle rests is as described by Sullivan et al. (2005) with an aerodynamic roughness length of 0.001 m (their intermediate estimate value), and 5) in the presence of large roughness the $m$ parameter in Eq. (1) is 0.7 as found by Gillies et al. (2007).

Another factor that needs be considered is the nature of the flow regime as defined by Lee and Soliman (1977) that would develop in the presence of the introduced roughness. According to Lee and Soliman (1977), the ratio of inter-row spacing length to element height will define whether the flow regime is isolated roughness flow, wake interference flow, or skimming flow. For all the roughness configurations used by Gillies et al. (2007) on Earth, this ratio is >4 indicating that the expected flow regime would be isolated roughness flow. A caveat to this is that on Earth the flow Reynolds number for all the tests of Gillies et al. (2007) was >24,000, and drag coefficients would be independent of $Re$. On Mars, this would likely not be the case for reasons described earlier.

## 5. Beta ($\beta$) effects on shear stress partitioning

On Mars the shear stress partitioning will be greatly affected by the dependency of the surface and element drag coefficients on Reynolds number. Assuming that in the presence of the roughness (i.e., the buckets placed in a staggered array on Mars) that $Cd_s$ is independent of $Re$, but that $Cd_e$ behaves as is shown in Fig. 1b, the relationship between the change in $\beta$ as a function of increasing regional shear stress and the partitioning of the stress for a surface with a λ value of 0.016 is shown in Fig. 2. The importance of the shear stress partitioning relationship is that it can be used to estimate the regional shear stress required to generate the threshold shear stress for particles of any given size lying on the intervening surface. For the case shown in Fig. 2 the regional shearing stress required to entrain a 125 μm diameter particle among the roughness would be 0.12 N $m^{-2}$, which is double the value (0.06 N $m^{-2}$) in the absence of the large roughness elements.

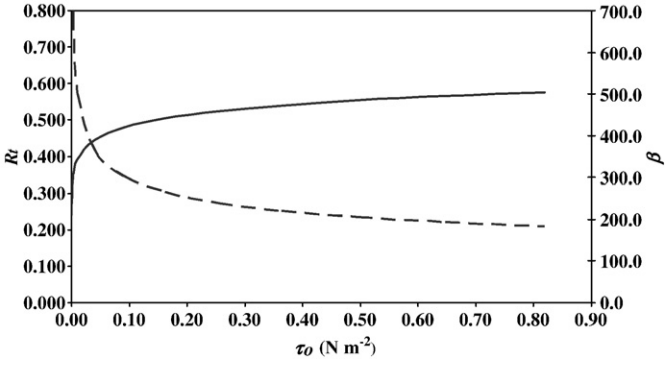


**Fig. 2.** The relationship between $\beta$ (dashed black line) changing as a function of increasing regional shear stress and the partitioning of the stress ($R_t$, solid black line) for a surface with a λ value of 0.016 assuming dependence of $Cd_e$ with $Re$.

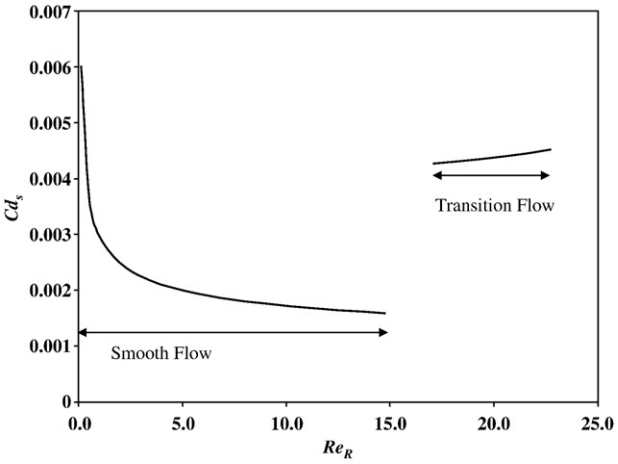


**Fig. 3.** Relationship between $Cd_S$ and $Re_R$ for the surface on Mars described by Sullivan et al. (2005), based on Kondo and Yamazawa (1986). The break in the curve represents the abrupt change in the roughness function at $Re_R\approx 17$ at the change from smooth flow to transition flow shown in Kondo and Yamazawa (1986), Fig. 4, p.129.

If we assume, based on Kondo and Yamazawa (1986), that $Cd_s$ is dependent on $Re_R$, and that the flow regime is isolated wake flow (Lee and Soliman, 1977), we could also assume that the intervening surface among the roughness elements (outside the wake zone behind an element) may respond as if no roughness was present. In this case $Cd_s$ would also change as a function of $Re_R$. Following Kondo and Yamazawa (1986), the relationship between $Cd_s$ and $Re_R$ for the surface previously identified (Sullivan et al., 2005) is shown in Fig. 3. To construct Fig. 3 we used the theoretical relationship for the smooth regime (i.e., $Re_R<17$) in which only skin friction dominates at a surface (i.e., Schlichting, 1979; Eq. (10) in Kondo and Yamazawa, 1986) and for the transitional roughness regime ($17<Re_R<63$) the data from Kondo and Yamazawa's (1986) Fig. 4 (p. 129) and their Eq. (9) (p. 128). A sudden change occurs in the relationship as the flow at the surface changes from aerodynamically smooth to transitional at $Re_R$ 10–17,

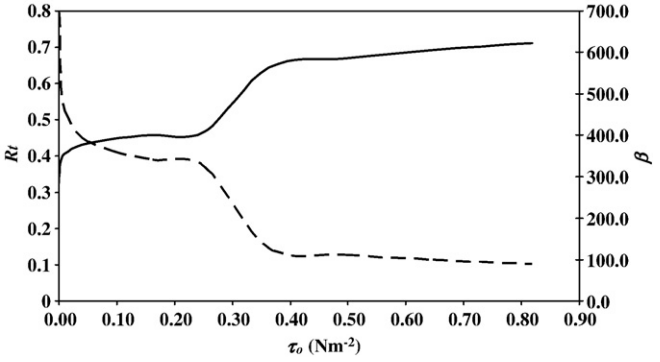


**Fig. 4.** The response of $\beta$ (dashed black line) and $R_t$ (solid black line) for the same $\lambda = 0.016$ surface if a dependence on $Cd_e$ on $Re$ and $Cd_s$ with $Re_R$ is assumed.

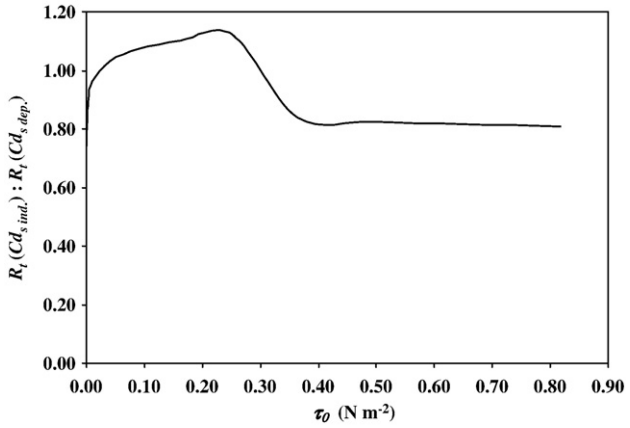


**Fig. 5.** The ratio of $R_t$ with $Cd_s$ independent of $Re_R$ and for the case where it is dependent on $Re_R$.

which creates a large change in $Cd_s$ as the roughness function ($R$) changes abruptly. If the relationship shown in Fig. 3 is combined with the element drag relationship shown in Fig. 1b, the response of the $\beta$ term becomes more complex and affects the $R_t$ relationship accordingly. The response of $\beta$ and $R_t$ for the dual Reynolds number dependency of the elements and the surface for the same $\lambda = 0.016$ surface is shown in Fig. 4.

The effect of including a $Cd_s$ dependent on $Re_R$ and the difference that results in the $R_t$ as compared to the case if $Cd_s$ was independent of $Re_R$ is shown in Fig. 5, expressed as the ratio between the two calculated $R_t$ values for each case, i.e., $Cd_s$ independent and $Cd_s$ dependent on $Re_R$. As regional $\tau_0$ increases, initially the ratio value is less than one (i.e., $R_t$ for the dependent $Cd_s$ condition is greater than for the static $Cd_s$) and it remains the case until the regional $\tau_0$ reaches $\approx 0.04$ N m$^{-2}$. As $Cd_s$ (dependent) decreases further with increasing $\tau_0$ the ratio exceeds one and increases until the flow changes to transitional. At this point $Cd_s$ begins to increase again, and the $\beta$ term decreases at a faster rate than if $Cd_s$ were constant and only $Cd_e$ were changing (i.e., Fig. 2), hence the ratio falls below one. At $\tau_0 = 0.36$ N m$^{-2}$, $R_t$ is approximately 15% lower in the case of $Cd_s$ independence from $Re_R$, which gradually increases to 20% lower at the limit of $\tau_0$ shown in Fig. 5.

## 6. Shear stress partitioning effects on entrainment threshold with increasing surface roughness

The detailed effects on particle entrainment threshold related to Reynolds number dependencies, as manifested through the $\beta$ term in Eq. (1), were described above for a particular $\lambda$ (i.e., 0.016). Assuming that the relationships for the surface and element drag coefficients remain the same as $\lambda$ increases (i.e., Figs. 1 and 3), the $R_t$ value at the regional shear stress (i.e., $\tau_0$) required to entrain a 125 μm particle on Mars with increasing $\lambda$ is shown in Fig. 6. For comparison purposes the relationships between threshold shear stress and $\lambda$ for the same 125 μm particle size on Earth are shown along with the cases of $Cd_s$ being independent of and dependent on $Re_R$ for Mars. At threshold little difference occurs in $R_t$ between the cases of $Cd_s$ being dependent or independent of $Re_R$. The difference in the shear stress ratio between the two cases increases with increasing $\tau_0$, as shown in Fig. 5.

Fig. 6 also shows that the high element drag coefficients associated with the roughness under Martian conditions results in much lower $R_t$ values than for the terrestrial condition, which means that for similar $\lambda$ values it requires much higher regional shear stresses on Mars to entrain the same sized particle. At a $\lambda$ of 0.016, the $R_t$ value is $\approx 33\%$ less on Mars than on Earth and at a $\lambda$ of 0.095 $\approx 46\%$ less. The question that can now be asked is "does the range of roughness described to this point have relevance to the Martian landscape?"

To our knowledge no estimates of $\lambda$ have been presented for Martian surfaces in the literature. Despite this, available data on the diameter and height of Martian surface rocks when coupled with data of unpublished rock number density (J.G. Ward, pers. comm.) provides a means to estimate values of $\lambda$ for select locations on Mars. Golombek and Rapp (1997) published data on the size frequency distribution of rocks at the Viking Lander 1 and 2 sites. Based on rock heights ($H$) and diameters ($D$) estimated from stereo-pair images made by the Viking Lander camera, they developed relationships for relating rock height to its diameter. Their generalized relationship between $H$ and $D$ (Eq. (15) in Golombek and Rapp, 1997) is:

$$H = (0.25 + 1.4k)D \tag{8}$$

where $k$ is used as a multiplier to change the $H$:$D$ relationship for relatively rock free areas ($k = 0.5$) and very rocky areas ($k = 0.3$).

Ward et al. (2005) presented size frequency and areal distribution of rock clasts at 13 traverses near the Spirit landing site, Gusev Crater, but they did not provide any data on rock height. They also did not include any estimates of the number of rocks in an area, but these data were made available by J.G. Ward to the authors in 2006. Two methods are applied to make estimates of rock heights at the Gusev crater site, which can then be combined with the rock number density to estimate $\lambda$ for Ward et al.'s (2005) transects. The first and simplest assumption is that the rock height is equivalent to its geometric mean diameter. A second estimate of rock height can be made by applying the $H$:$D$ relationship of Golombek and Rapp (1997) (Eq. (8)) to the geometric mean rock diameter data of Ward et al. (2005). The estimates of $\lambda$ for the 13 transects, made using both assumptions for calculating rock height, and that rock basal area can be represented by a circle and frontal area by diameter times height are shown in Table 1. Based on the assumptions made, the range of estimated $\lambda$ values for the Martian surfaces, described by Ward et al. (2005), falls within the range evaluated by Gillies et al. (2007) and used in the present study. Although it has been demonstrated that the size and shape of the roughness influences sediment transport (Gillies et al., 2006), the aerodynamics of the shear stress partitioning as a function of the roughness has been shown to be independent of its spatial distribution (Raupach et al., 2006; Brown et al., 2008), and perhaps weakly dependent on its height (King et al., 2008), so the estimates of regional threshold shear stress required to entrain 125 μm diameter particles from rough Martian surfaces (Fig. 6) should be reasonable and realistic, if one accepts that the model assumptions used are reasonable as well. The relationship of $R_t$ as a function of $\lambda$ can be developed for a range of sand-sized particles and a family of curves

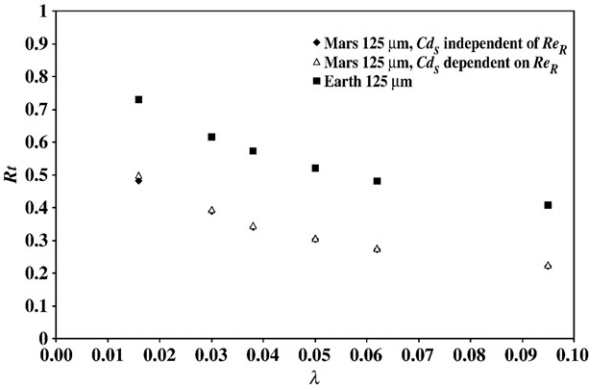


**Fig. 6.** The relationship between the shear stress ratio $R_t$ and $\lambda$ the roughness descriptor for a 125 μm diameter particle positioned among the roughness elements described by Gillies et al. (2007) for Earth (solid black squares) and on Mars (open triangles represent conditions where $Cd_s$ is dependent on $Re_h$, black diamonds represent conditions where $Cd_s$ is independent of $Re_h$, and in both cases $Cd_e$ is dependent on $Re$).

**Table 1**
Estimates of surface roughness density (λ) for Martian surfaces near Gusev crater described by Ward et al. (2005) using rock diameter and height relationships from Golombek and Rapp (1997).

| Image ID[a] | Rock density[b] (# $m^{-2}$) | Geo. mean diameter[a] (m) | Rock height (m) | $\lambda_{Geo.\ mean\ diameter}$ | Rock height based on Golombek and Rapp (1997) | | $\lambda_{G\&R}$[c] | $\lambda_{G\&R}$[d] |
|---|---|---|---|---|---|---|---|---|
| | | | | | $k=0.05$, rock "free"[c] | $k=0.30$, rocky area[d] | | |
| 2P127528536EFF0309P2364L7M1 | 450 | 0.0044 | 0.0044 | 0.009 | 0.0014 | | 0.00279 | |
| 2P129996790EFF0506P2599L7M1 | 2300 | 0.0063 | 0.0063 | 0.091 | | 0.0042 | | 0.0612 |
| 2P131335102EFF1151P2433L7M1 | 350 | 0.0075 | 0.0075 | 0.020 | 0.0024 | | 0.00630 | |
| 2P131873287EFF1300P2514R1M1 | 500 | 0.01 | 0.01 | 0.050 | 0.0032 | | 0.01600 | |
| 2P132134510EFF1500P2514R1M1 | 210 | 0.014 | 0.014 | 0.041 | 0.0045 | | 0.01317 | |
| 2P133016691EFF2100P2514R1M1 | 200 | 0.016 | 0.016 | 0.051 | 0.0051 | | 0.01638 | |
| 2P134088909EFF22FKP2514R1C1 | 1600 | 0.0053 | 0.0053 | 0.045 | | 0.0036 | | 0.0301 |
| 2P135415365EFF2900P2514R1C1 | 1500 | 0.005 | 0.005 | 0.038 | | 0.0034 | | 0.0251 |
| 2P135857093EFF3100P2514R1M1 | 570 | 0.011 | 0.011 | 0.069 | 0.0035 | | 0.0221 | |
| 2P136307457EFF3600P2514R1M1 | 1200 | 0.0065 | 0.0065 | 0.051 | | 0.0044 | | 0.0340 |
| 2P137011277EFF4000P2514R1M1 | 530 | 0.011 | 0.011 | 0.064 | 0.0035 | | 0.0205 | |
| 2P137636467EFF47DQP2514R1M1 | 1000 | 0.0073 | 0.0073 | 0.053 | | 0.0049 | | 0.0357 |
| 2P139318188EFF5800P2514R1M1 | 960 | 0.0075 | 0.0075 | 0.054 | 0.0024 | | 0.0173 | |

[a] Data from Ward et al. (2005) Table 1.
[b] Data from Ward (pers. comm., 2006).
[c] Rock density <1000 $m^{-2}$.
[d] Rock density >1000 $m^{-2}$.

developed for Martian conditions using the Raupach et al. (1993) shear stress partitioning model.

## 7. Probability of reaching entrainment threshold

With estimates of the shear stress ratio for surface of different λ it should be possible to evaluate the likelihood of reaching the entrainment threshold for particles if we had knowledge of the magnitude and frequency distribution of $\tau_0$ for different surfaces on Mars. These data or even data on the horizontal wind speed range on Mars, however, remain limited. Sutton et al. (1978) estimated Martian $u_*$ varies mostly between 0.4 and 0.6 m $s^{-1}$, which is insufficient for entrainment of sand-sized particles. Other authors (e.g., Arvidson et al., 1983; Moore, 1985; Sullivan et al., 2005) have estimated that $u_*$ during gusts in dust storms could reach values between 2.2 and 4.0 m $s^{-1}$. Indirect evidence, in the form of aeolian bedforms also suggests that threshold shear stress must be achieved periodically for these forms to have been created. Parteli and Herrmann (2007), based on modeling barchan dune formation in the Arkhangelsky crater, estimate that winds at some time must reach $u_*=3$ m $s^{-1}$.

The lower value of $u_*=2.2$ m $s^{-1}$ would not be sufficient to achieve entrainment threshold for a 125 μm diameter particle for surfaces with $\lambda>0.0046$. At the upper end of the range, $u_*=4.0$ m $s^{-1}$, entrainment could be achieved for surfaces with $\lambda\leq 0.068$, but surfaces with $\lambda>\approx 0.07$ should be stable and not subject to entrainment for this particle size. How often wind shear velocities reach these higher values on Mars is uncertain as well, but Arvidson et al. (1983) suggest winds on Mars sustain a $u_*=3.0$ m $s^{-1}$ for 40 s every five years. This indicates that the opportunity for rough surfaces to experience entrainment of sand-sized particles on Mars is less frequent than on Earth. Parteli and Herrmann (2007) reported that this very infrequent occurrence of high wind shear explains why imaging data from orbiting spacecraft have never revealed any significant movement of Martian dunes. The occurrence of entrainment thresholds being reached for sand-sized particles on rough surfaces would seem to have even less probability of occurrence, which decreases with increasing roughness because of shear stress partitioning effects.

## 8. Conclusions

Based on results presented by Gillies et al. (2007) that demonstrated that the Raupach et al. (1993) shear stress partitioning model showed very good agreement with measurements made at the full scale, the model was used to extrapolate how large surface roughness elements of different roughness density could influence entrainment thresholds of a known sand-size (125 μm diameter) on Mars. Application of the model to Martian atmospheric conditions suggests that on Mars shear stress partition is non-linear, with the shear stress ratio changing with regional shear stress for rough surfaces. This results from the dependency effects of the Reynolds number on the element and potentially the surface drag coefficients, which are expected to persist to at least the maximum reported wind speeds for Mars.

Shear stress partitioning effects will critically affect particle entrainment thresholds on Mars and complicate the threshold curves that have been published that describe the relationship between particle size and shear stress for smooth surfaces. Depending on the relationship between local roughness density and the nature of the shear stress partitioning (e.g., Fig. 6) a family of curves will be required to estimate the regional shear stresses required to entrain particles of a given size for a specific site on Mars. Consequently, developing regional sediment transport models, or relating sand transport to wind patterns produced by global or regional climate models will be a very complex exercise. In general, however, on Mars higher regional shear stresses are required to initiate particle entrainment for surfaces that have the same physical roughness as defined by the roughness density term (λ) compared with terrestrial surfaces mainly because of the low Martian atmospheric density.

## Acknowledgements

This research was funded, in part, through the NASA Mars Fundamental Research Program (Grant, NAG5-12759) and a NASA EPSCoR Grant to the Nevada System of Higher Education (Grant, NSHE 08-53). W.G. Nickling gratefully acknowledges the financial support of the Natural Sciences and Engineering Research Council of Canada (Grant 7427-02). The authors would also like to thank J.G. Ward for providing us with the rock density data for the Meridiani Planum landing site, which made it possible to estimate roughness density values for this area of Mars.

## References

Arvidson, R.E., Guinness, E.A., Moore, H.J., Tillman, J., Wall, S.D., 1983. Three Mars years: Viking Lander 1 imaging observations. Science 222, 463–468. doi:10.1126/science.222.4623.463.

Brown, S., Nickling, W.G., Gillies, J.A., 2008. A wind tunnel examination of shear stress partitioning for an assortment of surface roughness distributions. Journal of Geophysical Research, Earth Surface 113, F02S06. doi:10.1029/2007JF000790.
Cantor, B.A., James, P.B., Caplinger, M., Wolff, M.J., 2001. Martian dust storms: 1999 Mars Orbiter Camera observations. Journal of Geophysical Research 106 (E10), 23653–23688.
Gierasch, P.J., 1974. Martian dust storms. Review of Geophysics and Space Science 12, 730–734.
Gillette, D.A., 1999. A qualitative geophysical explanation for "hot spot" dust emitting source regions. Contributions to Atmospheric Physics 72 (1), 67–77.
Gillies, J.A., Nickling, W.G., King, J., 2006. Aeolian sediment transport through large patches of roughness in the atmospheric inertial sublayer. Journal of Geophysical Research, Earth Surface 111 (F02006). doi:10.1029/2005JF000434.
Gillies, J.A., Nickling, W.G., King, J., 2007. Shear stress partitioning in large patches of roughness in the atmospheric inertial sublayer. Boundary-Layer Meteorology 122 (2), 367–396.
Golombek, M., Rapp, D., 1997. Size-frequency distribution of rocks on Mars and Earth analog sites: implications for future landed missions. Journal of Geophysical Research 102, 4117–4129.
Greeley, R., White, B., Leach, R., Iversen, J., Pollack, J., 1976. Mars: wind friction speeds for particle movement. Geophysical Research Letters 3 (8), 417–420.
Greeley, R., Leach, R., White, B., Iversen, J., Pollack, J., 1980. Threshold windspeeds for sand on Mars: wind tunnel simulations. Geophysical Research Letters 7 (2), 121–124.
Hess, S.L., 1973. Martian winds and dust clouds. Planetary and Space Science 21, 1549–1557.
Iversen, J.D., White, B.R., 1982. Saltation threshold on Earth, Mars, and Venus. Sedimentology 29, 111–119.
Iversen, J., Pollack, J.B., Greeley, R., White, B.R., 1976. Saltation threshold on Mars: the effect of interparticle forces, surface roughness, and low atmospheric density. Icarus 29, 381–393.
Jackson, P.S., 1981. On the displacement height in the logarithmic velocity profile. Journal of Fluid Mechanics 111, 15–25.
Jakosky, B.M., Christensen, P.R., 1986. Are the Viking Lander site representative of Mars? Icarus 66, 125–133.
King, J., Nickling, W.G., Gillies, J.A., 2005. Representation of vegetation and other non-erodible elements in aeolian sediment transport models. Journal of Geophysical Research — Earth Surface 110 (F4), F04015. doi:10.1029/2004JF000281.
King, J., Nickling, W.G., Gillies, J.A., 2008. Investigations of the law-of-the-wall over sparse roughness elements. Journal of Geophysical Research, Earth-Surface 113, F02S07. doi:10.1029/2007JF000804.
Kondo, J., Yamazawa, H., 1986. Bulk transfer coefficient over a snow surface. Boundary-Layer Meteorology 34, 123–135.
Larsen, S.E., Jørgensen, H.E., Landberg, L., Tillman, J.E., 2002. Aspects of the atmospheric surface layer on Mars and Earth. Boundary —Layer Meteorology 105, 451–470.
Lee, B.E., Soliman, B.F., 1977. An investigation of the forces on three dimensional bluff bodies in rough wall turbulent boundary layers. Journal of Fluids Engineering 99, 503–510.
Leovy, C., 2001. Weather and climate on Mars. Nature 412, 245–249.
Lim, H.C., Castro, I.P., Hoxey, R.P., 2007. Bluff bodies in deep turbulent boundary layers: Reynolds-number issues. Journal of Fluid Mechanics 571, 97–118.
Mahrt, L., Vickers, D., Sun, J., Jensen, N., Jørgensen, H., Pardyjak, E., Fernando, H., 2001. Determination of the surface drag coefficient. Boundary-Layer Meteorology 99 (2), 249–276.
Martin, L.J., Zurek, R.W., 1993. An analysis of the history of dust activity on Mars. Journal of Geophysical Research 98 (E2), 3221–3246.
Moore, H.J., 1985. The Martian dust storm of Sol 1742. Journal of Geophysical Research 90, D163–D174 ISSN:0148–0227, Supplement.
Parteli, E.J.R., Herrmann, H.J., 2007. Dune formation on the present Mars. Physical Review E 76 (041307). doi:10.1103/PhysRevE.76.041307.
Prandtl, L., 1935. The mechanics of viscous fluids. In: Durand, F. (Ed.), Aerodynamic Theory. Springer-Verlag, Berlin, pp. 57–100.
Raupach, M.R., 1992. Drag and drag partition on rough surfaces. Boundary Layer Meteorology 60, 375–395.
Raupach, M.R., Gillette, D.A., Leys, J.F., 1993. The effect of roughness elements on wind erosion threshold. Journal of Geophysical Research 98 (D2), 3023–3029.
Raupach, M.R., Hughes, D.E., Cleugh, H.A., 2006. Momentum absorption in rough-wall boundary layers with sparse roughness elements in random and clustered distributions. Boundary-Layer Meteorology 120, 201–218. doi:10.1007/s10546-006-9058-4.
Sagan, C., Pollack, J., 1969. Wind blown dust on Mars. Nature 233, 791–794.
Schlichting, H., 1936. Experimentelle untersuchungen zum rauhigkeitsproblem. Ingenieur-Archiv 7, 1–34.
Schlichting, H., 1979. Boundary-Layer Theory, 7th ed. McGraw Hill, New York.
Stout, J.E., Zobeck, T.M., 1997. Intermittent saltation. Sedimentology 44 (5), 959–970.
Sullivan, R., 2002. Threshold-of-motion wind friction speeds at the Mars Pathfinder Landing site. XXXIII Annual Lunar and Planetary Science Conference. Lunar and Planetary Institute, Houston, Texas. Abstract #2022.
Sullivan, R., Banfield, D., Bell III, J.F., Calvin, W., Fike, D., Golombek, M., Greeley, R., Grotzinger, J., Herkenhoff, K., Jerolmack, D., Malin, M., Ming, D., Soderblom, L.A., Squyres, S.W., Thompson, S., Watters, W.A., Weitz, C.M., Yen, A., 2005. Aeolian processes at the Mars Exploration Rover Meridiani Planum landing site. Nature 436, 58–61.
Sutton, J.L., Leovy, C.B., Tillman, J.E., 1978. Diurnal variations of the Martian surface layer meteorological parameters during the first 45 Sols at two Viking Lander sites. Journal of the Atmospheric Sciences 35 (12), 2346–2355.
Thompson, A.M., Wilson, B.N., Hansen, B.J., 2004. Shear stress partitioning for idealized vegetated surfaces. Transactions of the American Association of Agricultural Engineers 47 (3), 701–709.
von Kármán, T., 1954. Aerodynamics Selected Topics in the Light of Their Historical Development. Cornell University Press, Ithaca, New York.
Ward, J.G., Arvidson, R.E., Golombek, M., 2005. The size-frequency and areal distribution of rock clasts at the Spirit landing site, Gusev Crater, Mars. Geophysical Research Letters 32 (L11203). doi:10.1029/2005GL022705.
Wolfe, S.A., Nickling, W.G., 1993. The protective role of sparse vegetation in wind erosion. Progress in Physical Geography 17, 50–68.